Highlights

- SIP-network analysis provided a direct link between interacting community members.
- Methanotrophic activity and community were resilient to desiccation-rewetting.
- Desiccation-rewetting structures the active interaction network.
- Interaction network became more complex but, less modular after disturbance.
- Legacy of disturbance persisted in the interaction network.

When the going gets tough: emergence of a complex methane-driven interaction network during recovery from desiccation-rewetting.

Thomas Kaupper[1], Lucas W. Mendes[2], Hyo Jung Lee[3], Yongliang Mo[4], Anja Poehlein[5], Zhongjun Jia[4], Marcus A. Horn[1]*, Adrian Ho[1]*.

[1]Institute for Microbiology, Leibniz Universität Hannover, Herrenhäuser Str. 2, 30419 Hannover, Germany.

[2]Center for Nuclear Energy in Agriculture, University of São Paulo CENA-USP, Brazil.

[3]Department of Biology, Kunsan National University, Gunsan, Republic of Korea.

[4]Institute of Soil Science, Chinese Academy of Sciences, No.71 East Beijing Road, Xuan-Wu District, Nanjing City, 210008 PR China.

[5]Department of Genomic and Applied Microbiology and Göttingen Genomics Laboratory, Institute of Microbiology and Genetics, George-August University Göttingen, Grisebachstr. 8, D-37077 Göttingen, Germany.

*For correspondence: Adrian Ho (adrian.ho@ifmb.uni-hannover.de), Marcus A. Horn (horn@ifmb.uni-hannover.de).

Running title: Response of a methane-driven interactome to disturbance.

Keywords: Stable-isotope probing / methane-based foodweb / community ecology / methanotrophs / *pmoA*.

Abstract

Microorganisms interact in complex communities, affecting microbially-mediated processes in the environment. Particularly, aerobic methanotrophs showed significantly stimulated growth and activity in the presence of accompanying microorganisms in an interaction network (interactome). Yet, little is known of how the interactome responds to disturbances, and how community functioning is affected by the disturbance-induced structuring of the interaction network. Here, we employed a time-series stable isotope probing (SIP) approach using ^{13}C-CH_4 coupled to a co-occurrence network analysis after Illumina MiSeq sequencing of the ^{13}C-enriched 16S rRNA gene to directly relate the response in methanotrophic activity to the network structure of the interactome after desiccation-rewetting of a paddy soil. Methane uptake rate decreased immediately (< 5 days) after short-term desiccation-rewetting. Although the methanotroph subgroups differentially responded to desiccation-rewetting, the metabolically active bacterial community composition, including the methanotrophs, recovered after the disturbance. However, the interaction network was profoundly altered, becoming more complex but, less modular after desiccation-rewetting, despite the recovery in the methanotrophic activity and community composition/abundances. This suggests that the legacy of the disturbance persists in the interaction network. The change in the network structure may have consequences for community functioning with recurring desiccation-rewetting.

1.0 Introduction

Biological interactions are widespread in microbial communities. Microorganisms form a plethora of interdependent relationships with their biotic environment, with synergistic and/or antagonistic effects. Concerning methanotrophy, emergent properties enhancing community functioning may arise from such interactions. Indeed, aerobic methanotrophs exhibit higher co-metabolic biodegradation rates of micropollutants and show significantly higher methanotrophic activity in a multi-species consortium than as monocultures (Begonja und Hrsak 2001; Ho et al. 2014; Benner et al. 2015; Krause et al. 2017; Veraart et al. 2018). Therefore, accompanying microorganisms that do not possess the metabolic potential and do not seemingly contribute to methane oxidation may also be relevant, exerting an indirect interaction-induced effect on community functioning. While changes in the methanotrophic community composition and/or abundances have been correlated to the methane oxidation rate in response to environmental cues and disturbances (Ho et al. 2011; Danilova et al. 2015; Christiansen et al. 2016; Reumer et al. 2018; Reis et al. 2020), interaction-induced effects that alter the structure of the interaction network (i.e., methanotrophic interactome; Ho et al. 2016a) remains unclear. Here, we define the methanotrophic interactome as a sub-population of the entire community, encompassing the methanotrophs and accompanying non-methanotrophs that is tracked *via* the flow of methane-derived ^{13}C; the members of the interactome co-occur more than by chance, as determined in a co-occurrence network analysis (Ho et al. 2016a). The recovery in the community composition and abundance does not necessarily translate to the return of the network structure to the pre-disturbance state (Pérez-Valera et al. 2017). Therefore, the response of the interactome is a lesser known but

important determinant, potentially imposing an effect on community functioning during recovery from disturbances (Ratzke et al. 2020).

Aerobic methanotrophs belong to the Gammaproteobacteria (Type Ia and Ib subgroups), Alphaproteobacteria (Type II subgroup), and Verrucomicrobia, and may show habitat preference (Knief 2015), with the verrucomicrobial methanotrophs typically inhabiting acidic and thermophilic geothermal environments (Op den Camp et al. 2009; Sharp et al. 2014). The proteobacterial methanotrophs are ubiquitous and thought to be relevant in terrestrial ecosystems, acting as a methane sink in well-aerated upland soils and methane biofilter at oxic-anoxic interfaces (Reim et al. 2012; Shrestha et al. 2012; Praeg et al. 2017; Ho et al. 2019; Kaupper et al. 2020a). Accordingly, proteobacterial methanotrophs can be distinguished based on their biochemistry and ecophysiology, which reflect on their ecological life strategies and response to disturbances (Trotsenko und Murrell 2008; Semrau et al. 2010; Ho et al. 2017). The *pmoA* gene (encoding for the particulate methane monooxygenase) phylogeny corresponds with that of the 16S rRNA gene, and is commonly targeted to characterize the methanotrophs in complex communities (e.g., Kolb et al. 2003; Dumont et al. 2011; Knief 2015; Karwautz et al. 2018). Therefore, aerobic methane oxidation is catalyzed by a defined microbial guild with relatively low diversity (mainly, proteobacteria in non-geothermal environments) when compared to other microbial groups catalyzing generalized processes (e.g., denitrification, respiration). This allows the methanotrophs to be clearly distinguished from the non-methanotrophs in complex communities, making the methanotrophic interactome a suitable model system for our study.

Here, we elaborate the response of a methane-driven interaction network to desiccation-rewetting to determine how methanotrophic activity is affected by the disturbance-induced structuring of the interactome. A DNA-based stable isotope probing (SIP) approach using ^{13}C-CH_4 was coupled to a co-occurrence network analysis after Illumina MiSeq sequencing of the 16S rRNA gene, allowing direct association of methanotrophic activity to the structure of the interaction network (methane food web). Although the network analysis is a useful tool to explore interactions in complex microbial communities (e.g., Barberán et al. 2012; Ho et al. 2016a; Morriën et al. 2017; Ho et al. 2020; Mo et al. 2020; Ratzke et al. 2020), biological interpretation of the analysis (e.g., causative mechanisms driving the interaction) requires further probing. Given that the methanotrophs are the only members of the interactome capable of using methane as a carbon and energy source, it is not unreasonable to assume that ^{13}C-labeled non-methanotrophic microorganisms depended on and interacted with the methanotrophs (e.g., *via* cross-feeding and co-aggregation; Ho et al. 2016a; Pérez-Valera et al. 2017). Coupling SIP to the network analysis thus confirms the unidirectional flow of substrate from the metabolically active methanotrophs to non-methanotrophs. We hypothesized that a more complex interaction network will arise as a response to desiccation-rewetting, as documented in other single or sporadic disturbance events, given sufficient recovery time (Eldridge et al. 2015; Pérez-Valera et al. 2017). With the elimination of less desiccation-resistant/tolerant microorganisms, it is not unreasonable to postulate that the surviving community members were forced to interact more among themselves, increasing metabolic exchange which further drives their co-occurrence over time (Zelezniak et al. 2015; Tripathi et al. 2016; Dal Co et al. 2020; Ratzke et al. 2020).

2.0 Materials and Methods

119

120 *2.1 Soil sampling and microcosm set-up*

121

122 The paddy soil (upper 10-15 cm) was collected from a rice field belonging to the Italian Rice
123 Research Institute, Vercelli, Italy (45° 20'N, 8° 25'W). The soil pH and electrical conductivity
124 (EC) were 6.5 and 0.2 dS m^{-1}, respectively. The C and N concentrations were 13.9 mg C g dw^{-1}
125 and 1.3 mg N g dw^{-1}, respectively. The concentrations of nitrite and nitrate (NO_x^-), sulphate,
126 and phosphate were 34.4 µg N g dw^{-1}, 96 µg g dw^{-1}, and 0.6 µg g dw^{-1}, respectively. Agricultural
127 practices in the rice field have been reported in detail elsewhere (Krueger et al. 2001).
128 Generally, rice was cropped in the paddy soil twice a year (May/June to September/October
129 and January/February to May/June), with each rice growing season spanning over 4-5 months;
130 rice was not grown for approximately two months in winter (Krueger et al. 2001). The paddy
131 field was drained prior to rice harvest and left fallow for 2-3 weeks before the commencement
132 of the next rice growing season. Soil sampling was performed in May 2015 after drainage and
133 rice harvest. After sampling, the soil was air-dried at ambient temperature and sieved (2 mm)
134 to eliminate (fine) roots and debris, before being stored in a plastic container at room
135 temperature till incubation set-up (November, 2017). Paddy soil prepared and stored under
136 the same conditions < 5 years after sampling showed comparable potentially active
137 methanotrophic community composition (mRNA-based community analysis) over ~ 80 days
138 incubation after re-wetting (Collet et al. 2015).

139

140 Each microcosm consisted of 10 g soil saturated with 4.5 mL autoclaved deionized water in a
141 Petri dish. The saturated soil was homogenized, and pre-incubated under ~10 $\%_{v/v}$ methane in
142 air at 25°C in an air-tight jar. Following pre-incubation (7 days), desiccation was induced by

143 placing the microcosms under a laminar flow cabinet overnight (15 hours) to achieve a
144 gravimetric water loss of > 95 % in the disturbed microcosm (Figure S1; Ho et al. 2016c). After
145 desiccation, water loss was replenished by adding the corresponding amount of autoclaved
146 deionized water, and incubation resumed under the same conditions as before. Microcosms
147 not exposed to desiccation-rewetting (un-disturbed) served as reference. A total of 42
148 microcosms were constructed (Figure S1). At designated intervals (i.e., pre-incubation, as well
149 as 1 – 7, 27 – 34, and 64 – 71 days after disturbance; Figure S1), ^{13}C-CH_4 labelling incubation
150 was performed; the microcosms (n=6) were transferred into a flux chamber and incubated
151 under 2 $\%_{v/v}$ methane (^{13}C-CH_4, n=4; $^{unlabelled}C$-CH_4, n=2) in air. Headspace methane was
152 replenished when methane in the flux chamber was reduced to < 0.5 $\%_{v/v}$. Incubation in the
153 flux chamber was performed over 6 - 7 days or until at least 500 µmole methane was
154 consumed to ensure sufficient labelling (Neufeld et al. 2007). After incubation, the soil was
155 homogenized, shock-frozen, and stored in the -20°C freezer until DNA extraction.
156
157 *2.2 Methane and inorganic N measurements.*
158
159 Headspace methane was measured daily in all replicates (i.e., both $^{unlabelled}C$- and ^{13}C-CH_4
160 incubations) using a gas chromatograph (7890B GC System, Agilent Technologies, Santa Clara,
161 USA) coupled to a pulsed discharge helium ionization detector (PD-HID), with helium as the
162 carrier gas. The methane uptake rates were determined by linear regression from the slope of
163 methane depletion with at least three time intervals (12-24 hours between intervals). Soluble
164 ammonium and nitrate were determined in all replicates in autoclaved deionized water
165 (1:2.5$_{w/v}$) after centrifugation and filtration (0.2 µm) of the soil suspension. Soluble ammonium
166 was determined colorimetrically (Horn et al. 2005) using an Infinite M plex plate reader

(TECAN, Meannedorf, Switzerland), whereas nitrate was determined using a Sievers 208i NO analyzer system (GE Analytical Instruments, Boulder, CO, USA) with 50 mM VCl_3 in 1 M sterile HCl as a reducing agent.

2.3 DNA extraction and isopycnic ultracentrifugation

DNA was extracted using the DNeasy PowerSoil Kit (Qiagen, Hilden, Germany) according to the manufacturer's instruction. DNA was extracted in duplicate for each sample (n=6, per treatment and time) and pooled after elution to obtain sufficient amounts for the isopycnic ultracentrifugation.

DNA stable isotope probing was performed according to Neufeld et al. (2007). Isopycnic ultracentrifugation was performed at 144000 g for 67 hours using an Optima L-80XP (Beckman Coulter Inc., USA). Each ultracentrifugation run consisted of DNA extracted from incubations containing ^{13}C- and ^{unlabelled}C-methane to distinguish the `light‘ from the `heavy` fractions (Figure S2). Fractionation was performed immediately after centrifugation using a hydraulic pump (Duelabo, Dusseldorf, Germany) at 3 rpm min^{-1}. Although 10 - 11 fractions were obtained, the last fraction was discarded, yielding 9 - 10 fractions per sample. Fractionation was unsuccessful for DNA sampled from two of the four replicate in the disturbed microcosm (^{13}C-CH_4 incubation, 64 - 71 days interval). Given that a minimum of three replicates is needed to construct each network, post-disturbance samples were grouped into days 1 - 7 (immediately after disturbance) and 27 – 71 (during recovery) for subsequent ^{13}C-enriched 16S rRNA gene-derived network analysis (see Section 2.7). In the other time intervals, at least three replicates were obtained in the ^{13}C-CH_4 incubation. The density gradient of each fraction

was determined by weighing on a precision scale (technical replicate, n=10). DNA precipitation was performed over night, as described in Neufeld et al. (2007); nucleic acid was washed twice with ethanol, and the pellet was suspended in 30 µL of ultrapure PCR water (INVITROGEN, Waltham, USA). The *pmoA* gene was enumerated from each fraction using a qPCR assay (MTOT; Table S1) to distinguish the 'heavy' from the 'light' fraction after comparing DNA from the ^{13}C- and $^{unlabelled}C$-CH_4 incubations (Figure S2). The identified 'heavy' and 'light' DNA fractions as defined in Neufeld et al. (2007) were amplified for Illumina MiSeq sequencing.

2.4 Group-specific qPCR assays.

The qPCR assays (MBAC, MCOC, and TYPEII targeting type Ia, Ib, and II, respectively) were performed to follow the abundance of the methanotroph sub-groups over time (Table S1). Additionally, a qPCR assay targeting the total methanotrophic population (MTOT) was applied to the DNA samples after fractionation to distinguish the 'heavy' from the 'light' fraction. The qPCR was performed using a BIORAD CFX Connect RT System (Biorad, Hercules, USA). Briefly, each reaction (total volume, 20 µL) consisted of 10 µL SYBR 2X Sensifast (BIOLINE, London, UK), 3.5 µL of forward/reverse primer each, 1 µL 0.04% BSA, and 2 µL template DNA. Template DNA was diluted 50-fold with RNase- and DNase-free water for the MBAC, MCOC, and TYPEII assays, and was undiluted for the MTOT assay. Diluting the template DNA 50-fold resulted in the optimal *pmoA* gene copy numbers. The primer combinations and concentrations, as well as the PCR thermal profiles, are given elsewhere (see Table S1, Kolb et al. 2003 and Kaupper et al. 2020b). The calibration curve (10^1-10^8 copy number of target genes) was derived from gene libraries as described before (Ho et al. 2011). The qPCR amplification efficiency was 83 – 91%, with R^2 ranging from 0.994 - 0.997. Amplicon specificity was determined from the melt

curve, and confirmed by 1% agarose gel electrophoresis yielding a band of the correct size in a preliminary qPCR run.

2.5 Amplification for the pmoA and 16S rRNA genes for Illumina MiSeq sequencing.

The *pmoA* gene was amplified using the primer pair A189f/mb661r, with the forward primer containing a fused 6 bp bar code. Each PCR reaction comprised of 25 µl SYBR Premix Ex Taq™ (Tli RNaseH Plus, TaKaRa, Japan), 1 µl forward/reverse primer each (10 µM), 2 µl template DNA (DNA concentration diluted to 2-8 ng μl^{-1}), and 21 µl sterilized distilled water, giving a total volume of 50 µl. The PCR thermal profile consisted of an initial denaturation step at 94 °C for 2 min, followed by 39 cycles of denaturation at 94°C for 30 s, annealing at 60°C for 30 s, and elongation at 72°C for 45 s. The final elongation step was at 72°C for 5 mins. The PCR products were verified on 1.2% agarose gel electrophoresis showing a single band of the correct size, before purification using the E.Z.N.A. Cycle-Pure kit (Omega Bio-tek, USA). Subsequently, the purified amplicons were pooled at equimolar DNA amounts (200 ng) for sequencing using Illumina MiSeq version 3 chemistry (paired-end, 600 cycles). The *pmoA* sequence library was prepared using the TruSeq Nano DNA LT Sample Prep Kit set A (Illumina, Beijing, China).

The 16S rRNA gene was amplified using the primer pair 341F/805R. Each PCR reaction comprised of 4 µl Buffers B and S each (CRYSTAL Taq-DNA-Polymerase, BiolabProducts, Germany), 4 µl $MgCl_2$ (25 mM), 0.2 µl Taq polymerase (5 U μl^{-1}) (CRYSTAL Taq-DNA-Polymerase), 1.6 µl dNTPs (10 mM), 2 µl forward and reverse tagged-primers each (10 µM), 4 µl template DNA, and 18.2 µl sterilized distilled water. The PCR thermal profile consisted of an

initial denaturation step at 94°C for 7 min, followed by 30 cycles of denaturation at 94°C for 30 s, annealing at 53°C for 30 s, and elongation at 72°C for 30 s. The final elongation step was at 72°C for 5 mins. After the specificity of the amplicon was checked by 1% agarose gel electrophoresis, the PCR product was purified using the GeneRead Size Selection Kit (Qiagen, Hilden, Germany). Subsequently, a second PCR was performed with adapters using the Nextera XT Index Kit (Illumina, San Diego, USA). The second PCR reaction consisted of 12.5 µl 2X KAPA HiFi HotStart Ready Mix (Roche, Mannheim, Germany), 2.5 µl of each tagged primers (10 µM), 2.5 µl PCR grade water, and 5 µl template from the first PCR. The amplicons were then purified using the MagSi-NGS^{PREP} Plus Magnetic beads (Steinbrenner Laborsysteme GmbH, Wiesenbacj, Germany). Normalization of the amplicons before sequencing was performed using the Janus Automated Workstation (Perkin Elmer, Waltham Massachusetts, USA). Sequencing was performed using Illumina MiSeq version 3 chemistry (paired-end, 600 cycles).

2.6 pmoA and 16S rRNA gene amplicon analyses

The *pmoA* gene amplicon was analyzed as described before (Reumer et al. 2018). Briefly, the paired-end reads were sorted based on the length and the quality of the primers (≤ 2 errors) and barcodes (≤ 1 error) after assembly in Mothur version 1.42.1 using the `make.contigs` command (Schloss et al. 2009). Primers and barcodes which did not meet these requirements were removed. Similarly, chimeric reads were also removed in Mothur using the `chimera.uchime` command with the `self` option. After filtering, the initial ~ 1 175 000 contigs generated from Illumina Miseq sequencing was reduced to ~ 628 000 high quality contigs, with approximately 15 300 contigs per sample. The *pmoA* sequences were classified using

BLAST by comparing to the GenBank nonredundant (nr) database and the lowest common ancestor algorithm in MEGAN version 5.11.3, based on curated *pmoA* gene database and MEGAN tree, respectively as detailed in Dumont et al. (2014). The high quality *pmoA* sequences could be affiliated (family, genus, or species level) to known cultured methanotrophs. Based on the relative abundance of the *pmoA* gene sequences, a principal component analysis (PCA) was performed to determine the response of the methanotrophs to desiccation-rewetting. To construct the PCA, the data matrix was initially analyzed using the detrended correspondence analysis (DCA), which indicated linearly distributed data and revealed that the best-fit mathematical model was the PCA. To test whether the treatments harbored significantly different bacterial community composition and structure, plot clustering was tested using permutational multivariate analysis of variance (PERMANOVA; Anderson 2001). The PCA was conducted in Canoco 4.5 (Biometrics, Wageningen, The Netherlands), and the PERMANOVA was calculated using PAST 4 software (Hammer et al. 2001). The *pmoA* gene sequences were deposited at the National Center for Biotechnology Information (NCBI), SRA database under the BioProject accession number PRJNA634611.

The 16S rRNA gene paired-end reads were firstly merged using PEAR (Zhang et al. 2014). Next, the merged sequences were processed using QIIME 2 version 2019.10, with de-multiplex and quality control performed with DADA2 (Callahan 2017) using the consensus method to remove any remaining chimeric and low-quality sequences. Approximately 1 300 000 high quality contigs were retained after filtering (on average, ~18 000 contigs per sample). After the removal of singletons and doubletons, the samples were rarefied to 7,560 sequences following the number of the lowest sample. The taxonomic affiliation was performed at 97% similarity according to the Silva database v. 132 (Quast et al. 2013). The affiliations of the OTUs

are given to the finest taxonomic resolution, whenever available. A PCA was performed to compare the bacterial community composition in the un-disturbed and disturbed incubations. The 16S rRNA-based PCA was constructed as described for the *pmoA*-based PCA using Canoco 4.5 (Biometrics, Wageningen, the Netherlands) after analysis of variance (PERMANOVA) in the PAST 4 software. The 16S rRNA gene sequences were deposited at the NCBI, SRA database under the BioProject accession number PRJNA634611.

2.7 Co-occurrence network analysis.

To explore the complexity of the interaction between bacterial taxa (OTU-level) within the interactome, a co-occurrence network analysis was performed based on the 16S rRNA gene derived from the ^{13}C-enriched DNA (`heavy´ fraction). For network construction, non-random co-occurrence analyses between bacterial OTUs were calculated using SparCC, a tool designed to assess correlations for compositional data (Friedman und Alm 2012). For each network, *P*-values were obtained by 99 permutations of random selections of the data tables, applying the same analytical pipeline. The true SparCC correlations were selected based on statistical significance of $p < 0.01$, with a magnitude of > 0.7 or < -0.7. The networks were assessed based on their topological features such as the number of nodes and edges (connectivity), modularity, number of communities, average path length, network diameter, average degree, and clustering coefficient (Table 1; Newman 2003). The nodes in the networks represent OTUs, whereas the edges represent significantly positive or negative correlations between two nodes. Also, key nodes were identified based on the betweenness centrality, a measure of the frequency of a node acting as a bridge along the shortest path between two other nodes (Poudel et al. 2016). Hence, nodes with high betweenness centrality can be regarded to

represent important key taxa within the interaction network (Borgatti 2005). The co-occurrence network analysis was performed using the Python module 'SparCC', and the network construction and properties were calculated with Gephi (Bastian et al. 2009).

2.8 Statistical analysis

Significant differences ($p<0.05$) in the methane uptake rate and qPCR analyses per time between treatments (un-disturbed and disturbed incubations) were performed using IBM SPSS Statistics (IBM, Armonk, USA). The data were tested for normal distribution using the Kolmogorov-Smirnov test and the Shapiro-Wilk test. Where normal distribution was met, a two-sided paired t-test was performed. Otherwise, a non-parametric test (Wilcoxon signed rank test) was performed. Additionally, methane uptake rates were correlated to the abundances of type Ia, Ib, and II *pmoA* gene separately by linear regression in Origin (OriginLab Corporation, Northampton, MA, USA).

3.0 Results

3.1 The abiotic environment.

The trend in methane uptake was largely comparable in the un-disturbed and disturbed incubations, where activity peaked at 27 – 34 days before reaching similar rates after 71 days (Figure 1). However, methane uptake was significantly lower ($p<0.05$) immediately after desiccation-rewetting when compared to the un-disturbed incubation (un-disturbed, 0.64 ±

0.06 µmol h^{-1} g dw^{-1}; desiccated-rewetted, 0.5 ± 0.05 µmol h^{-1} g dw^{-1}); the adverse effects of the disturbance on methane uptake were transient (< 5 days).

Soluble ammonium and nitrate were rapidly consumed during pre-incubation (Figure S3). The inorganic N concentrations significantly increased ($p<0.05$) after desiccation-rewetting. However, the elevated inorganic N concentrations were not sustained. Soluble ammonium and nitrate concentrations decreased to values similar to those after pre-incubation at ~34 days. Particularly, ammonium concentration was significantly higher in the un-disturbed than in the disturbed microcosm after incubation (day 71).

3.2 Response in methanotroph abundance.

Group-specific qPCR assays were performed to enumerate the *pmoA* genes belonging to type Ia, Ib, and II methanotrophs to be used as proxies for methanotrophic abundances. Generally, the gammaproteobacterial methanotrophs were less responsive to desiccation-rewetting than the alphaproteobacterial ones (Figure 2). Although values were within the same order of magnitude and the discrepancies documented were not appreciable, changes in the abundance of type Ia and Ib methanotrophs were statistically significant comparing the un-disturbed to the desiccation-rewetted microcosms. Consistently, like for the type II methanotrophs, methane uptake rates were significantly ($p<0.05$) correlated to the abundances of type Ib methanotrophs (Figure S4). It is also noteworthy that type I methanotrophs were appreciably more abundant in the disturbed microcosm after the incubation despite showing an adverse effect on population numbers soon after desiccation-rewetting (Figure 2). Particularly, the type II methanotroph abundance recovered well,

appreciably increased by around two orders of magnitude after desiccation-rewetting (7 – 71 days). By comparison, type I methanotroph abundance also increased but within a relatively narrow range (type Ia methanotrophs, 2.1 x 10^7 ± 7.4 x 10^6 to 3.4 x 10^7 ± 7.0 x 10^6; type Ib methanotrophs, 2.5 x 10^7 ± 7.9 x 10^6 to 1.9 x 10^8 ± 6.6 x 10^7 gene copy numbers g dw soil^{-1}) during the same time frame (Figure 2). It appears that although type II methanotrophs constitute a minor overall fraction of the methanotrophic population, they were more responsive and significantly increased in abundance after desiccation-rewetting.

3.3 Effects of desiccation-rewetting on the methanotrophic community composition, as determined by DNA-based SIP.

The bacterial communities, including the methanotrophs in the 'heavy' and 'light' fractions were distinct, as revealed in a PCA for each time interval, showing a clear separation of the ^{13}C-enriched and ^{unlabelled}C-DNA (Figure S5). The 16S rRNA- and *pmoA* gene-derived sequencing analyses were then performed on the ^{13}C-enriched DNA, representing the metabolically active and replicating community. The *pmoA* gene was sequenced before (after pre-incubation) and immediately after disturbance (1 – 7 days interval), as well as after incubation (64 – 71 days interval) to follow the recovery of the methanotrophic community composition. The *pmoA* gene sequences, visualized as a PCA (Figure 3), revealed a distinct active methanotrophic community prior to the disturbance (pre-incubation), and the community shifted soon after desiccation-rewetting, diverging from the community in the un-disturbed microcosm. Over 96 % of the variation in the methanotrophic community composition could be explained by PC1 and PC2 (67.9 % and 28.5 % of the total variance, respectively). The active methanotrophs which emerged soon after desiccation-rewetting (1 – 7 days interval) were predominantly

comprised of members belonging to the putative Rice Paddy Cluster (RPC) closely affiliated to *Methylocaldum* (type Ib; Lüke et al. 2014; Shiau et al. 2018). 71 days post-desiccation-rewetting, the recovering community in the disturbed, as well as in the un-disturbed microcosms were more scattered, largely comprising of type I methanotrophs. The active methanotrophs showed dynamic population shifts after desiccation-rewetting, with the recovered community becoming more varied after incubation.

3.4 Effects of desiccation-rewetting on the total bacterial community composition, as determined by DNA-based SIP.

The active bacterial community was largely comprised of members belonging to Gammaproteobacteria (families Methylomonaceae, Methylophilaceae, Burkholderiaceae, Rhodocyclaceae, and Nitrosomonadaceae), Bacteroidetes (family Chitinophagaceae and Microscillaceae), and Gemmatimonadetes (family Gemmatimonadaceae), collectively representing the majority of the population (> 75 %; Figure 4). Like the *pmoA* gene sequence analysis, the PCA derived from the 16S rRNA gene sequences revealed a compositional shift in the bacterial community after desiccation-rewetting, but the community recovered after 71 days, closely resembling the composition in the un-disturbed microcosm (Figure 3). Comparing the community in the un-disturbed and disturbed microcosms, *Methylocaldum* (type Ib methanotroph), and *Methylobacter* (type Ia) as well as members of Burkholderiaceae, were respectively detected at appreciably higher relative abundance soon after desiccation-rewetting (1-7 days interval) and during recovery (27-71 days interval), consistent with the *pmoA* gene sequence analysis (Figure S6). The active members of the bacterial community in the un-disturbed microcosm were generally more diverse; microorganisms present at

406 differentially higher relative abundances belonged to Proteobacteria, Bacteroidetes,
407 Verrucomicrobia, and Acidobacteria (family/genus level identification, Figures 4 and S6).
408 Generally, the *pmoA* and 16S rRNA gene sequencing analyses were consistent, revealing the
409 compositional shift and recovery of the active community.
410
411 *3.5 Response of the co-occurrence network structure to desiccation-rewetting.*
412
413 A 16S rRNA gene-based co-occurrence network analysis derived from the ^{13}C-enriched `heavy`
414 fraction was performed to explore the complexity of the methane-driven interactome
415 immediately after, and during the recovery from desiccation-rewetting (resilience; Figure 5).
416 These networks were assessed by their topological properties comparing the un-disturbed
417 and disturbed incubations (Table 1). Generally, both the microbial communities in the un-
418 disturbed and after desiccation-rewetting increased in connectivity over time (i.e., higher no.
419 of edges, degree, clustering coefficient; Table 1). However, a more connected network
420 emerged after desiccation-rewetting (> 27 days), exhibiting a higher number of connections
421 (edges), connections per node (degree), and clustering coefficient than in the un-disturbed
422 community (Table 1). Accordingly, the desiccation-rewetted community was characterized by
423 a shorter average path length (Table 1). Although modularity generally decreased in all
424 microcosms after pre-incubation, the community showed a less modular structure after
425 desiccation-rewetting when compared to the un-disturbed community during recovery.
426 Additionally, to account for biases arising from the imbalance number of replicates used to
427 construct the networks (i.e., grouping of 27-34 and 64-71 days intervals yielding a higher
428 number of replicates, n= 6 or 7), the networks were re-constructed using 4 randomly selected
429 replicates from all replicates for the 27-71 days interval. The results obtained were consistent

and support the general trends documented in the networks using all replicates (Table S2). Overall, the network structure of the active bacterial community became more complex and connected after recovery from desiccation-rewetting, demonstrating that the disturbance fostered a closer association of community members within the interactome.

The top five nodes with the highest betweenness centrality were identified in all treatments (Figure 5 & Table S3). As anticipated, the key nodes comprised of methanotrophs, as well as non-methanotrophic methylotrophs; the methanotrophs are a subset of the methylotrophs (Chistoserdova 2015). Surprisingly, many other non-methanotrophic bacterial taxa also formed the key nodes. These taxa were rather unique to each treatment (un-disturbed and disturbed) at 1-7 and 27 – 71 days intervals (Figure 5 & Table S3). It appears that non-methanotrophs, albeit unable to assimilate methane directly, were also relevant members of the interactome.

4.0 Discussion

4.1 Recovery and resilience of the methanotrophic activity and community composition following desiccation-rewetting.

The methanotrophic activity was resilient to desiccation-rewetting. Periodic exposure of the paddy soil to lower soil water content after drainage for rice harvest may have selected for a desiccation-tolerant methanotrophic community. This may partly explain the transient (<5 days) adverse effect on methane uptake rates, which rapidly recovered. Nevertheless, the recovery in methanotrophic activity to single disturbance events is not entirely unexpected,

454 as has been shown before (e.g., soil structural disruption, (Kumaresan et al. 2011); long-term
455 drought spanning over decades, (Collet et al. 2015); desiccation and heat stress, (Ho et al.
456 2016c; 2016b). Similarly, methanotrophic activity recovered from multiple disturbances, with
457 soils harboring low-affinity methanotrophs showing resilience to repeated desiccation and
458 ammonium stress (van Kruistum et al. 2018), and compounded disturbances associated to
459 land transformation given sufficient recovery time (e.g., over 15 years after peat excavation;
460 Reumer et al. 2018). However, the recovery in methane oxidation may be accompanied by
461 compositional shifts in the methanotrophic community, affecting the trajectory of
462 methanotroph succession after disturbance (Ho et al. 2016c).
463
464 In contrast to previous work (e.g., Kumaresan et al. 2011; Collet et al. 2015; Ho et al. 2016c;
465 Jurburg et al. 2017; Krause et al. 2017; Ho et al. 2018; Reumer et al. 2018), a time-series ^{13}C-
466 CH_4 labeling approach was employed in this study to directly relate not only the
467 methanotrophic activity to the response of the metabolically active methanotrophs, but also
468 to the structure of the interaction network, to desiccation-rewetting. The active bacterial
469 community composition, including the methanotrophs, recovered well as indicated by the 16S
470 rRNA gene sequence analysis, which showed that the disturbed community resembled that of
471 the un-disturbed community, clustering closely together after incubation (PCA; Figure 3).
472 Specifically, *Methylocaldum* was predominant soon after desiccation-rewetting, whereas
473 *Methylobacter* and Burkholderiaceae were present at relatively higher abundances during
474 recovery from the disturbance (Figures 4 and S6). Gammaproteobacterial methanotrophs,
475 including *Methylocaldum* and *Methylobacter* species, are generally known to be rapid
476 colonizers, proliferating under high nutrient and methane availability (Ho et al. 2013; Ho et al.
477 2016b), whereas the dominance and role of Burkholderiaceae during recovery from

disturbances remain elusive. However, members of the family Burkholderiaceae exhibit metabolic versatility, with *Cupriavidus* reported to stimulate methanotrophic growth (Stock et al. 2013). Furthermore, *Ralstonia*, another Burkholderiaceae, has been documented to co-occur with methanotrophs in a ^{13}C-CH_4 labeling study, likely caused by cross-feeding, suggesting that there was a trophic interaction with methanotrophs (Qiu et al. 2008). Like for the gammaproteobacterial type Ib methanotrophs, the significant correlation between methane uptake rates and the alphaproteobacterial methanotrophs suggests a coupling of methanotrophic activity and the growth of these methanotrophic sub-groups (Figure S4). The alphaproteobacterial methanotrophs (*Methylocystis;* type II) were seemingly more responsive to the disturbance, exhibiting a gradual increase in numerical abundance during the incubation (Figure 2). This reinforces previous studies documenting the emergence of this sub-group (*Methylocystis-Methylosinus*) after stress events (Ho et al. 2011; Ho et al. 2016c; 2016b; van Kruistum et al. 2018). It is thought that desiccation-rewetting may trigger the proliferation of alphaproteobacterial methanotrophs either by awakening dormant members of the seedbank community and/or generating open niches for recolonization (Whittenbury et al. 1970; Collet et al. 2015; Ho et al. 2016b; Kaupper et al. 2020b). Also, the gradual increase in alphaproteobacterial methanotroph abundance may be attributable to a relatively slower recovery after being adversely affected by desiccation-rewetting, having a lower initial abundance than gammaproteobacterial methanotrophs. Admittedly, we cannot exclude experimental artifacts deriving from soil preparation which may affect the methanotrophs, but the soil was mildly pre-processed (i.e., air-dried at ambient temperature and sieved), ensuring homogeneity for a standardized incubation. Overall, the differential response among methanotroph sub-groups was consistent with trends detected previously.

4.2 The emergence of a more complex and connected methane-driven interactome after desiccation-rewetting.

Methanotrophs thrive in the presence of specific accompanying microorganisms, exhibiting higher activity and growth as cocultures than as monocultures (Iguchi et al. 2011; Stock et al. 2013; Ho et al. 2014; Jeong et al. 2014; Benner et al. 2015; Krause et al. 2017; Veraart et al. 2018). This emphasizes the relevance of interdependent relationships among members of a methanotrophic interactome for community functioning. Although methanotrophic activity and community composition may recover, disturbances may exert an impact on the structure of the microbial network, affecting the interaction among community members which may have consequences in future disturbances (Berg und Ellers 2010; Bissett et al. 2013; Sun et al. 2013; Ho et al. 2020; Ratzke et al. 2020).

Interestingly, the methanotrophic interactome became more complex and increased in connectivity during recovery (> 27 days) from desiccation-rewetting (Table 1 & Figure 5). The disturbance-induced highly connected interactome suggests higher competition for specific niches (van Elsas et al. 2012), which likely became available after the disturbance event. This enables rapid re-colonization of the open niches, resulting in the recovery of methanotrophic activity and abundance, particularly when methane is not limiting (Ho et al. 2011; Pan et al. 2014; Kaupper et al. 2020b). The emergence of a more complex network after disturbance also suggests that the loss of some microorganisms were compensated by other community members having similar roles; the community was thus sufficiently redundant to sustain methanotrophic activity (Eldridge et al. 2015; Mendes et al. 2015; Tripathi et al. 2016). Similarly, when compared to an un-perturbed soil, the bacterial network after bio-

perturbation (> 12 months) caused by the foraging activity of burrowing mammals increased in connectedness (Eldridge et al. 2015). In another form of disturbance, the microbial network was altered, increasing in the number of positively co-occurring bacteria during the recovery from a forest fire (12 months; Pérez-Valera et al. 2017). In line with these studies, the interaction networks increased in complexity, becoming more connected after deforestation for oil palm (Tripathi et al. 2016) and after abandonment of agriculture (Morriën et al. 2017).

Like these disturbances, desiccation-rewetting fostered closer associations among interacting members of the methanotrophic interactome, supporting our hypothesis. The increase in network complexity, as indicated by a higher number of edges, degree, and clustering efficiency suggests a more connected network, concomitant to a shorter average path length which indicates a tighter and more efficient network, in response to desiccation-rewetting (Zhou et al. 2010; Mendes et al. 2018; Dal Co et al. 2020). Hence, desiccation-rewetting likely augmented or consolidated metabolic exchange to increase co-occurrence among community members within the interactome, giving rise to a more complex interaction network (Zelezniak et al. 2015; Ratzke et al. 2020). The increase in network complexity directly related to the recovery in methanotrophic activity. Nevertheless, modularity decreased over time, possessing fewer independently connected groups (compartments) within the network (Zhou et al. 2010), more pronounced in the desiccation-rewetted community. A highly modular network is thought to restrict and localize the effects of a disturbance within compartments in the network (Ruiz-Moreno et al. 2006; Zhou et al. 2010). Therefore, the loss of modularity after contemporary disturbances suggests that future disturbances will more evenly affect community members. Hence, community composition and activity, when examined alongside

549 the network structure, provided a more comprehensive understanding of microbial responses
550 to contemporary and future disturbances.
551
552 Expectedly, the nodes with high betweenness centrality were found to comprise of
553 methylotrophs, including the methanotrophs (Figure 5). These key nodes were not necessarily
554 bacterial taxa that were present at significantly higher relative abundances (e.g.,
555 Burkholderiaceae; Figure 4) but rather, refer to nodes acting as a bridge between other nodes
556 with significantly higher frequencies (Poudel et al. 2016). As such, the key nodes within the
557 network are crucial members of the methanotrophic interactome, potentially having a
558 significant regulatory effect on the other members of the interactome; the loss of the key
559 nodes is anticipated to unravel the interaction network (Williams et al. 2014; van der Heijden
560 and Hartmann 2016). Because the methylotrophs can oxidize methanol and other
561 intermediary products of methane oxidation (e.g., formaldehyde, formate), cross-feeding
562 between the methanotrophs and non-methanotrophic methylotrophs (e.g., *Methylotenera*,
563 *Methylophilus*) drives their co-occurrence, as has been established before (Krause et al. 2017).
564 Interestingly, many non-methanotrophs/methylotrophs also formed the key nodes. Given
565 that the non-methanotrophs cannot utilize methane as a carbon and energy source, their
566 identification as key nodes indicates their potential regulatory role, indirectly *via* interaction-
567 induced effects, on the methanotrophic activity (van der Heijden and Hartmann 2016). Among
568 the non-methanotrophic key nodes, other members of Sphingomonadaceae (*Sphingopyxis*)
569 but not specifically *Sphingomonas*, have been shown to significantly stimulate the expression
570 of the *pmoA* gene when co-cultured with an alphaproteobacterial methanotroph
571 (*Methylocystis*; Jeong et al. 2014). Members of Gemmatimonadaceae have been co-detected
572 along with the methanotrophs in ^{13}C-CH_4 labelling SIP studies, but their exact role within the

interacome remains to be elucidated (Zheng et al. 2014). Similarly, the underlying mechanisms that drive the interaction between other co-occurring bacterial taxa and the methanotrophs warrant further exploration through isolation and co-culture studies (Kwon et al. 2018). However, it is likely that some members of the co-occurring taxa may reciprocally interact with the methanotrophs, supporting methanotrophic growth and activity (e.g., *Sphingomonas*), and contributed to the resilience of the methanotrophs following desiccation-rewetting. Accordingly, the bacterial taxa representing key nodes were distinct in the un-disturbed microcosm and after desiccation-rewetting, despite compositional recovery among metabolically active members of the community (Figure 3). This indicates sufficient redundancy among active members of the methanotrophic interactome; presumably, the different key taxa in the un-disturbed and disturbed community shared similar traits relevant for community functioning.

4.3 Conclusion

Our findings, based on the time-resolved ^{13}C-CH_4 SIP approach, reinforced previous DNA-based studies, showing the differential response among the methanotrophs to disturbances, likely reflecting on their ecological life strategies (Ho et al. 2013). Widening current understanding, we showed that although methanotrophic activity recovered after desiccation-rewetting and the post-disturbance microbial community may resemble those in the un-disturbed soil, the disturbance legacy manifests in the structure of the co-occurrence network, which became more complex but less modular. Therefore, community interaction profoundly changed after desiccation-rewetting, which may have consequences for community functioning with recurring and/or compounded disturbances. More generally, our

findings move beyond biodiversity-ecosystem functioning relationships to encompass interaction-induced responses in community functioning.

Acknowledgements

We are grateful to Stefanie Hetz and Daria Frohloff for excellent research assistance. TK and AH are financially supported by the Deutsche Forschungsgemeinschaft (grant no. HO6234/1-1). AH and MAH are also financially supported by the Leibniz Universität Hannover, Germany.

All authors declare that they have no conflict of interest.

All authors have seen and approved the final version submitted.

References

Anderson, Marti J. (2001): A new method for non-parametric multivariate analysis of variance. In: *Austral Ecology* 26 (1), S. 32–46. DOI: 10.1111/j.1442-9993.2001.01070.pp.x.

Barberán, Albert; Bates, Scott T.; Casamayor, Emilio O.; Fierer, Noah (2012): Using network analysis to explore co-occurrence patterns in soil microbial communities. In: *The ISME journal* 6 (2), S. 343–351. DOI: 10.1038/ismej.2011.119.

Bastian, M.; Heymann, S.; Jacomy, M. (2009): Gephi: An Open Source Software for Exploring and Manipulating Networks. In: *In International AAAI Conference on Weblogs and Social Media* (8), S. 361–362.

Begonja, A.; Hrsak, D. (2001): Effect of Growth Conditions on the Expression of Soluble Methane Monooxygenase. In: *Food technology and biotechnology* (39 (1)), S. 29–35.

Benner, Jessica; Smet, Delfien de; Ho, Adrian; Kerckhof, Frederiek-Maarten; Vanhaecke, Lynn; Heylen, Kim; Boon, Nico (2015): Exploring methane-oxidizing communities for the co-metabolic degradation of organic micropollutants. In: *Applied microbiology and biotechnology* 99 (8), S. 3609–3618. DOI: 10.1007/s00253-014-6226-1.

Berg, Matty P.; Ellers, Jacintha (2010): Trait plasticity in species interactions: a driving force of community dynamics. In: *Evol Ecol* 24 (3), S. 617–629. DOI: 10.1007/s10682-009-9347-8.

Bissett, Andrew; Brown, Mark V.; Siciliano, Steven D.; Thrall, Peter H. (2013): Microbial community responses to anthropogenically induced environmental change: towards a systems approach. In: *Ecology letters* 16 Suppl 1, S. 128–139. DOI: 10.1111/ele.12109.

Borgatti, Stephen P. (2005): Centrality and network flow. In: *Social Networks* 27 (1), S. 55–71. DOI: 10.1016/j.socnet.2004.11.008.

Callahan, Benjamin (2017): Rdp Taxonomic Training Data Formatted For Dada2 (Rdp Trainset 16/Release 11.5).

Chistoserdova, Ludmila (2015): Methylotrophs in natural habitats: current insights through metagenomics. In: *Applied microbiology and biotechnology* 99 (14), S. 5763–5779. DOI: 10.1007/s00253-015-6713-z.

Christiansen, Jesper Riis; Levy-Booth, David; Prescott, Cindy E.; Grayston, Sue J. (2016): Microbial and Environmental Controls of Methane Fluxes Along a Soil Moisture Gradient in a Pacific Coastal Temperate Rainforest. In: *Ecosystems* 19 (7), S. 1255–1270. DOI: 10.1007/s10021-016-0003-1.

Collet, Sebastian; Reim, Andreas; Ho, Adrian; Frenzel, Peter (2015): Recovery of paddy soil methanotrophs from long term drought. In: *Soil Biology and Biochemistry* 88, S. 69–72. DOI: 10.1016/j.soilbio.2015.04.016.

Dal Co, Alma; van Vliet, Simon; Kiviet, Daniel Johannes; Schlegel, Susan; Ackermann, Martin (2020): Short-range interactions govern the dynamics and functions of microbial communities. In: *Nature ecology & evolution* 4 (3), S. 366–375. DOI: 10.1038/s41559-019-1080-2.

Danilova, O. V.; Belova, S. E.; Kulichevskaya, I. S.; Dedysh, S. N. (2015): Decline of activity and shifts in the methanotrophic community structure of an ombrotrophic peat bog after wildfire. In: *Microbiology* 84 (5), S. 624–629. DOI: 10.1134/S0026261715050045.

651 Dumont, Marc G.; Lüke, Claudia; Deng, Yongcui; Frenzel, Peter (2014): Classification of pmoA
652 amplicon pyrosequences using BLAST and the lowest common ancestor method in MEGAN. In:
653 *Front. Microbiol.* 5. DOI: 10.3389/fmicb.2014.00034.

654 Dumont, Marc G.; Pommerenke, Bianca; Casper, Peter; Conrad, Ralf (2011): DNA-, rRNA- and mRNA-
655 based stable isotope probing of aerobic methanotrophs in lake sediment. In: *Environmental*
656 *microbiology* 13 (5), S. 1153–1167. DOI: 10.1111/j.1462-2920.2010.02415.x.

657 Eldridge, David J.; Woodhouse, Jason N.; Curlevski, Nathalie J. A.; Hayward, Matthew; Brown, Mark
658 V.; Neilan, Brett A. (2015): Soil-foraging animals alter the composition and co-occurrence of
659 microbial communities in a desert shrubland. In: *The ISME journal* 9 (12), S. 2671–2681. DOI:
660 10.1038/ismej.2015.70.

661 Friedman, Jonathan; Alm, Eric J. (2012): Inferring correlation networks from genomic survey data. In:
662 *PLoS computational biology* 8 (9), e1002687. DOI: 10.1371/journal.pcbi.1002687.

663 Hammer, Ø.; Harper, D.A.T.; Ryan, P.D (2001): PAST: Paleontological statistics software package for
664 education and data analysis. In: *Palaeontologia Electronica* (4(1)), 9pp.

665 Ho, Adrian; Angel, Roey; Veraart, Annelies J.; Daebeler, Anne; Jia, Zhongjun; Kim, Sang Yoon et al.
666 (2016a): Biotic Interactions in Microbial Communities as Modulators of Biogeochemical
667 Processes: Methanotrophy as a Model System. In: *Frontiers in microbiology* 7, S. 1285. DOI:
668 10.3389/fmicb.2016.01285.

669 Ho, Adrian; Di Lonardo, D. Paolo; Bodelier, Paul L. E. (2017): Revisiting life strategy concepts in
670 environmental microbial ecology. In: *FEMS microbiology ecology* 93 (3). DOI:
671 10.1093/femsec/fix006.

672 Ho, Adrian; Kerckhof, Frederiek-Maarten; Luke, Claudia; Reim, Andreas; Krause, Sascha; Boon, Nico;
673 Bodelier, Paul L. E. (2013): Conceptualizing functional traits and ecological characteristics of
674 methane-oxidizing bacteria as life strategies. In: *Environmental microbiology reports* 5 (3), S. 335–
675 345. DOI: 10.1111/j.1758-2229.2012.00370.x.

676 Ho, Adrian; Lee, Hyo Jung; Reumer, Max; Meima-Franke, Marion; Raaijmakers, Ciska; Zweers, Hans et
677 al. (2019): Unexpected role of canonical aerobic methanotrophs in upland agricultural soils. In:
678 *Soil Biology and Biochemistry* 131, S. 1–8. DOI: 10.1016/j.soilbio.2018.12.020.

679 Ho, Adrian; Lüke, Claudia; Cao, Zhihong; Frenzel, Peter (2011): Ageing well: methane oxidation and
680 methane oxidizing bacteria along a chronosequence of 2000 years. In: *Environmental*
681 *microbiology reports* 3 (6), S. 738–743. DOI: 10.1111/j.1758-2229.2011.00292.x.

682 Ho, Adrian; Lüke, Claudia; Reim, Andreas; Frenzel, Peter (2016b): Resilience of (seed bank) aerobic
683 methanotrophs and methanotrophic activity to desiccation and heat stress. In: *Soil Biology and*
684 *Biochemistry* 101, S. 130–138. DOI: 10.1016/j.soilbio.2016.07.015.

685 Ho, Adrian; Mendes, Lucas W.; Lee, Hyo Jung; Kaupper, Thomas; Mo, Yongliang; Poehlein, Anja et al.
686 (2020): Response of a methane-driven interaction network to stressor intensification. submitted.
687 In: *FEMS microbiology ecology* 96 (10). DOI: 10.1093/femsec/fiaa180.

688 Ho, Adrian; Mo, Yongliang; Lee, Hyo Jung; Sauheitl, Leopold; Jia, Zhongjun; Horn, Marcus A. (2018):
689 Effect of salt stress on aerobic methane oxidation and associated methanotrophs; a microcosm
690 study of a natural community from a non-saline environment. In: *Soil Biology and Biochemistry*
691 125, S. 210–214. DOI: 10.1016/j.soilbio.2018.07.013.

Ho, Adrian; Roy, Karen de; Thas, Olivier; Neve, Jan de; Hoefman, Sven; Vandamme, Peter et al. (2014): The more, the merrier: heterotroph richness stimulates methanotrophic activity. In: *The ISME journal* 8 (9), S. 1945–1948. DOI: 10.1038/ismej.2014.74.

Ho, Adrian; van den Brink, Erik; Reim, Andreas; Krause, Sascha M. B.; Bodelier, Paul L. E. (2016c): Recurrence and Frequency of Disturbance have Cumulative Effect on Methanotrophic Activity, Abundance, and Community Structure. In: *Frontiers in microbiology* 6, S. 1493. DOI: 10.3389/fmicb.2015.01493.

Horn, Marcus A.; Ihssen, Julian; Matthies, Carola; Schramm, Andreas; Acker, Georg; Drake, Harold L. (2005): Dechloromonas denitrificans sp. nov., Flavobacterium denitrificans sp. nov., Paenibacillus anaericanus sp. nov. and Paenibacillus terrae strain MH72, N2O-producing bacteria isolated from the gut of the earthworm Aporrectodea caliginosa. In: *International journal of systematic and evolutionary microbiology* 55 (Pt 3), S. 1255–1265. DOI: 10.1099/ijs.0.63484-0.

Iguchi, Hiroyuki; Yurimoto, Hiroya; Sakai, Yasuyoshi (2011): Stimulation of methanotrophic growth in cocultures by cobalamin excreted by rhizobia. In: *Applied and environmental microbiology* 77 (24), S. 8509–8515. DOI: 10.1128/AEM.05834-11.

Jeong, So-Yeon; Cho, Kyung-Suk; Kim, Tae Gwan (2014): Density-dependent enhancement of methane oxidation activity and growth of Methylocystis sp. by a non-methanotrophic bacterium Sphingopyxis sp. In: *Biotechnology reports (Amsterdam, Netherlands)* 4, S. 128–133. DOI: 10.1016/j.btre.2014.09.007.

Jurburg, Stephanie D.; Nunes, Inês; Brejnrod, Asker; Jacquiod, Samuel; Priemé, Anders; Sørensen, Søren J. et al. (2017): Legacy Effects on the Recovery of Soil Bacterial Communities from Extreme Temperature Perturbation. In: *Frontiers in microbiology* 8, S. 1832. DOI: 10.3389/fmicb.2017.01832.

Karwautz, Clemens; Kus, Günter; Stöckl, Michael; Neu, Thomas R.; Lueders, Tillmann (2018): Microbial megacities fueled by methane oxidation in a mineral spring cave. In: *The ISME journal* 12 (1), S. 87–100. DOI: 10.1038/ismej.2017.146.

Kaupper, Thomas; Hetz, Stefanie; Kolb, Steffen; Yoon, Sukhwan; Horn, Marcus A.; Ho, Adrian (2020a): Deforestation for oil palm: impact on microbially mediated methane and nitrous oxide emissions, and soil bacterial communities. In: *Biol Fertil Soils* 56 (3), S. 287–298. DOI: 10.1007/s00374-019-01421-3.

Kaupper, Thomas; Luehrs, Janita; Lee, Hyo Jung; Mo, Yongliang; Jia, Zhongjun; Horn, Marcus A.; Ho, Adrian (2020b): Disentangling abiotic and biotic controls of aerobic methane oxidation during re-colonization. In: *Soil Biology and Biochemistry* 142, S. 107729. DOI: 10.1016/j.soilbio.2020.107729.

Knief, Claudia (2015): Diversity and Habitat Preferences of Cultivated and Uncultivated Aerobic Methanotrophic Bacteria Evaluated Based on *pmoA* as Molecular Marker. In: *Frontiers in microbiology* 6, S. 1346. DOI: 10.3389/fmicb.2015.01346.

Kolb, S.; Knief, C.; Stubner, S.; Conrad, R. (2003): Quantitative Detection of Methanotrophs in Soil by Novel pmoA-Targeted Real-Time PCR Assays. In: *Applied and environmental microbiology* 69 (5), S. 2423–2429. DOI: 10.1128/AEM.69.5.2423-2429.2003.

Krause, Sascha M. B.; Johnson, Timothy; Samadhi Karunaratne, Yasodara; Fu, Yanfen; Beck, David A. C.; Chistoserdova, Ludmila; Lidstrom, Mary E. (2017): Lanthanide-dependent cross-feeding of

methane-derived carbon is linked by microbial community interactions. In: *Proceedings of the National Academy of Sciences of the United States of America* 114 (2), S. 358–363. DOI: 10.1073/pnas.1619871114.

Krueger, Martin; Frenzel, Peter; Conrad, Ralf (2001): Microbial processes influencing methane emission from rice fields. In: *Global Change Biol* 7 (1), S. 49–63. DOI: 10.1046/j.1365-2486.2001.00395.x.

Kumaresan, Deepak; Stralis-Pavese, Nancy; Abell, Guy C. J.; Bodrossy, Levente; Murrell, J. Colin (2011): Physical disturbance to ecological niches created by soil structure alters community composition of methanotrophs. In: *Environmental microbiology reports* 3 (5), S. 613–621. DOI: 10.1111/j.1758-2229.2011.00270.x.

Kwon, Miye; Ho, Adrian; Yoon, Sukhwan (2018): Novel approaches and reasons to isolate methanotrophic bacteria with biotechnological potentials: recent achievements and perspectives. In: *Applied microbiology and biotechnology*. DOI: 10.1007/s00253-018-9435-1.

Lüke, Claudia; Frenzel, Peter; Ho, Adrian; Fiantis, Dian; Schad, Peter; Schneider, Bellinda et al. (2014): Macroecology of methane-oxidizing bacteria: the β-diversity of pmoA genotypes in tropical and subtropical rice paddies. In: *Environmental microbiology* 16 (1), S. 72–83. DOI: 10.1111/1462-2920.12190.

Mendes, Lucas W.; Tsai, Siu M.; Navarrete, Acácio A.; Hollander, Mattias de; van Veen, Johannes A.; Kuramae, Eiko E. (2015): Soil-borne microbiome: linking diversity to function. In: *Microbial ecology* 70 (1), S. 255–265. DOI: 10.1007/s00248-014-0559-2.

Mendes, Lucas William; Raaijmakers, Jos M.; Hollander, Mattias de; Mendes, Rodrigo; Tsai, Siu Mui (2018): Influence of resistance breeding in common bean on rhizosphere microbiome composition and function. In: *The ISME journal* 12 (1), S. 212–224. DOI: 10.1038/ismej.2017.158.

Mo, Yongliang; Jin, Feng; Zheng, Yan; Baoyin, Taogetao; Ho, Adrian; Jia, Zhongjun (2020): Succession of bacterial community and methanotrophy during lake shrinkage. In: *J Soils Sediments* 20 (3), S. 1545–1557. DOI: 10.1007/s11368-019-02465-6.

Morriën, Elly; Hannula, S. Emilia; Snoek, L. Basten; Helmsing, Nico R.; Zweers, Hans; Hollander, Mattias de et al. (2017): Soil networks become more connected and take up more carbon as nature restoration progresses. In: *Nature communications* 8, S. 14349. DOI: 10.1038/ncomms14349.

Neufeld, Josh D.; Vohra, Jyotsna; Dumont, Marc G.; Lueders, Tillmann; Manefield, Mike; Friedrich, Michael W.; Murrell, J. Colin (2007): DNA stable-isotope probing. In: *Nat Protoc* 2 (4), S. 860–866. DOI: 10.1038/nprot.2007.109.

Newman, M. E. J. (2003): The Structure and Function of Complex Networks. In: *SIAM Rev.* 45 (2), S. 167–256. DOI: 10.1137/S003614450342480.

Op den Camp, Huub J. M.; Islam, Tajul; Stott, Matthew B.; Harhangi, Harry R.; Hynes, Alexander; Schouten, Stefan et al. (2009): Environmental, genomic and taxonomic perspectives on methanotrophic Verrucomicrobia. In: *Environmental microbiology reports* 1 (5), S. 293–306. DOI: 10.1111/j.1758-2229.2009.00022.x.

Pan, Yao; Abell, Guy C. J.; Bodelier, Paul L. E.; Meima-Franke, Marion; Sessitsch, Angela; Bodrossy, Levente (2014): Remarkable recovery and colonization behaviour of methane oxidizing bacteria

in soil after disturbance is controlled by methane source only. In: *Microbial ecology* 68 (2), S. 259–270. DOI: 10.1007/s00248-014-0402-9.

Pérez-Valera, Eduardo; Goberna, Marta; Faust, Karoline; Raes, Jeroen; García, Carlos; Verdú, Miguel (2017): Fire modifies the phylogenetic structure of soil bacterial co-occurrence networks. In: *Environmental microbiology* 19 (1), S. 317–327. DOI: 10.1111/1462-2920.13609.

Poudel, R.; Jumpponen, A.; Schlatter, D. C.; Paulitz, T. C.; Gardener, B. B. McSpadden; Kinkel, L. L.; Garrett, K. A. (2016): Microbiome Networks: A Systems Framework for Identifying Candidate Microbial Assemblages for Disease Management. In: *Phytopathology* 106 (10), S. 1083–1096. DOI: 10.1094/PHYTO-02-16-0058-FI.

Praeg, Nadine; Wagner, Andreas O.; Illmer, Paul (2017): Plant species, temperature, and bedrock affect net methane flux out of grassland and forest soils. In: *Plant Soil* 410 (1-2), S. 193–206. DOI: 10.1007/s11104-016-2993-z.

Qiu, Qiongfen; Noll, Matthias; Abraham, Wolf-Rainer; Lu, Yahai; Conrad, Ralf (2008): Applying stable isotope probing of phospholipid fatty acids and rRNA in a Chinese rice field to study activity and composition of the methanotrophic bacterial communities in situ. In: *The ISME journal* 2 (6), S. 602–614. DOI: 10.1038/ismej.2008.34.

Quast, Christian; Pruesse, Elmar; Yilmaz, Pelin; Gerken, Jan; Schweer, Timmy; Yarza, Pablo et al. (2013): The SILVA ribosomal RNA gene database project: improved data processing and web-based tools. In: *Nucleic acids research* 41 (Database issue), D590-6. DOI: 10.1093/nar/gks1219.

Ratzke, Christoph; Barrere, Julien; Gore, Jeff (2020): Strength of species interactions determines biodiversity and stability in microbial communities. In: *Nature ecology & evolution* 4 (3), S. 376–383. DOI: 10.1038/s41559-020-1099-4.

Reim, Andreas; Lüke, Claudia; Krause, Sascha; Pratscher, Jennifer; Frenzel, Peter (2012): One millimetre makes the difference: high-resolution analysis of methane-oxidizing bacteria and their specific activity at the oxic-anoxic interface in a flooded paddy soil. In: *The ISME journal* 6 (11), S. 2128–2139. DOI: 10.1038/ismej.2012.57.

Reis, Paula C. J.; Thottathil, Shoji D.; Ruiz-González, Clara; Prairie, Yves T. (2020): Niche separation within aerobic methanotrophic bacteria across lakes and its link to methane oxidation rates. In: *Environmental microbiology* 22 (2), S. 738–751. DOI: 10.1111/1462-2920.14877.

Reumer, Max; Harnisz, Monika; Lee, Hyo Jung; Reim, Andreas; Grunert, Oliver; Putkinen, Anuliina et al. (2018): Impact of Peat Mining and Restoration on Methane Turnover Potential and Methane-Cycling Microorganisms in a Northern Bog. In: *Applied and environmental microbiology* 84 (3). DOI: 10.1128/AEM.02218-17.

Ruiz-Moreno, D.; Pascual, M.; Riolo, R. (2006): Exploring network space with genetic algorithms: modularity, resilience and reactivity. In: l.M. Pascua und J. A. Dunne (Hg.): Ecological Networks: Linking Structure to Dynamics In Food Webs. New York, NY: Oxford University Press, S. 187–208.

Schloss, Patrick D.; Westcott, Sarah L.; Ryabin, Thomas; Hall, Justine R.; Hartmann, Martin; Hollister, Emily B. et al. (2009): Introducing mothur: open-source, platform-independent, community-supported software for describing and comparing microbial communities. In: *Applied and environmental microbiology* 75 (23), S. 7537–7541. DOI: 10.1128/AEM.01541-09.

Semrau, Jeremy D.; DiSpirito, Alan A.; Yoon, Sukhwan (2010): Methanotrophs and copper. In: *FEMS Microbiol Rev* 34 (4), S. 496–531. DOI: 10.1111/j.1574-6976.2010.00212.x.

817 Sharp, Christine E.; Smirnova, Angela V.; Graham, Jaime M.; Stott, Matthew B.; Khadka, Roshan;
818 Moore, Tim R. et al. (2014): Distribution and diversity of Verrucomicrobia methanotrophs in
819 geothermal and acidic environments. In: *Environmental microbiology* 16 (6), S. 1867–1878. DOI:
820 10.1111/1462-2920.12454.

821 Shiau, Yo-Jin; Cai, Yuanfeng; Jia, Zhongjun; Chen, Chi-Ling; Chiu, Chih-Yu (2018): Phylogenetically
822 distinct methanotrophs modulate methane oxidation in rice paddies across Taiwan. In: *Soil*
823 *Biology and Biochemistry* 124, S. 59–69. DOI: 10.1016/j.soilbio.2018.05.025.

824 Shrestha, Pravin Malla; Kammann, Claudia; Lenhart, Katharina; Dam, Bomba; Liesack, Werner (2012):
825 Linking activity, composition and seasonal dynamics of atmospheric methane oxidizers in a
826 meadow soil. In: *The ISME journal* 6 (6), S. 1115–1126. DOI: 10.1038/ismej.2011.179.

827 Stock, Michiel; Hoefman, Sven; Kerckhof, Frederiek-Maarten; Boon, Nico; Vos, Paul de; Baets,
828 Bernard de et al. (2013): Exploration and prediction of interactions between methanotrophs and
829 heterotrophs. In: *Research in Microbiology* 164 (10), S. 1045–1054. DOI:
830 10.1016/j.resmic.2013.08.006.

831 Sun, Melanie Y.; Dafforn, Katherine A.; Johnston, Emma L.; Brown, Mark V. (2013): Core sediment
832 bacteria drive community response to anthropogenic contamination over multiple environmental
833 gradients. In: *Environmental microbiology* 15 (9), S. 2517–2531. DOI: 10.1111/1462-2920.12133.

834 Tripathi, Binu M.; Edwards, David P.; Mendes, Lucas William; Kim, Mincheol; Dong, Ke; Kim, Hyoki;
835 Adams, Jonathan M. (2016): The impact of tropical forest logging and oil palm agriculture on the
836 soil microbiome. In: *Molecular ecology* 25 (10), S. 2244–2257. DOI: 10.1111/mec.13620.

837 Trotsenko, Yuri A.; Murrell, John Colin (2008): Metabolic Aspects of Aerobic Obligate Methanotrophy.
838 In: Allen I. Laskin, Geoffrey M. Gadd und Sima Sariaslani (Hg.): Advances in applied microbiology.
839 Vol. 63, Bd. 63. 1st ed. Amsterdam: Academic Press (Advances in applied microbiology), S. 183–
840 229.

841 van der Heijden, Marcel G. A.; Hartmann, Martin (2016): Networking in the Plant Microbiome. In:
842 *PLoS biology* 14 (2), e1002378. DOI: 10.1371/journal.pbio.1002378.

843 van Elsas, Jan Dirk; Chiurazzi, Mario; Mallon, Cyrus A.; Elhottova, Dana; Kristufek, Václav; Salles,
844 Joana Falcão (2012): Microbial diversity determines the invasion of soil by a bacterial pathogen.
845 In: *Proceedings of the National Academy of Sciences of the United States of America* 109 (4), S.
846 1159–1164. DOI: 10.1073/pnas.1109326109.

847 van Kruistum, Henri; Bodelier, Paul L. E.; Ho, Adrian; Meima-Franke, Marion; Veraart, Annelies J.
848 (2018): Resistance and Recovery of Methane-Oxidizing Communities Depends on Stress Regime
849 and History; A Microcosm Study. In: *Frontiers in microbiology* 9, S. 1714. DOI:
850 10.3389/fmicb.2018.01714.

851 Veraart, A. J.; Garbeva, P.; van Beersum, F.; Ho, A.; Hordijk, C. A.; Meima-Franke, M. et al. (2018):
852 Living apart together-bacterial volatiles influence methanotrophic growth and activity. In: *The*
853 *ISME journal* 12 (4), S. 1163–1166. DOI: 10.1038/s41396-018-0055-7.

854 Whittenbury, R.; Davies, S. L.; Davey, J. F. (1970): Exospores and cysts formed by methane-utilizing
855 bacteria. In: *Journal of General Microbiology* 61 (2), S. 219–226. DOI: 10.1099/00221287-61-2-
856 219.

857 Williams, Ryan J.; Howe, Adina; Hofmockel, Kirsten S. (2014): Demonstrating microbial co-occurrence
858 pattern analyses within and between ecosystems. In: *Frontiers in microbiology* 5, S. 358. DOI:
859 10.3389/fmicb.2014.00358.

860 Zelezniak, Aleksej; Andrejev, Sergej; Ponomarova, Olga; Mende, Daniel R.; Bork, Peer; Patil, Kiran
861 Raosaheb (2015): Metabolic dependencies drive species co-occurrence in diverse microbial
862 communities. In: *Proceedings of the National Academy of Sciences of the United States of*
863 *America* 112 (20), S. 6449–6454. DOI: 10.1073/pnas.1421834112.

864 Zhang, Jiajie; Kobert, Kassian; Flouri, Tomáš; Stamatakis, Alexandros (2014): PEAR: a fast and
865 accurate Illumina Paired-End reAd mergeR. In: *Bioinformatics (Oxford, England)* 30 (5), S. 614–
866 620. DOI: 10.1093/bioinformatics/btt593.

867 Zheng, Y.; Huang, R.; Wang, B. Z.; Bodelier, P. L. E.; Jia, Z. J. (2014): Competitive interactions between
868 methane- and ammonia-oxidizing bacteria modulate carbon and nitrogen cycling in paddy soil. In:
869 *Biogeosciences* 11 (12), S. 3353–3368. DOI: 10.5194/bg-11-3353-2014.

870 Zhou, Jizhong; Deng, Ye; Luo, Feng; He, Zhili; Tu, Qichao; Zhi, Xiaoyang (2010): Functional molecular
871 ecological networks. In: *mBio* 1 (4). DOI: 10.1128/mBio.00169-10.

872

873

874

875

876

877 **Table 1:** Correlations and topological properties of the interaction networks during pre-

878 incubation, and recovery from desiccation-rewetting at 1 - 7 and 27 - 71 days intervals.

879

Network properties	Pre-incubation	Un-disturbed		Disturbed	
		1-7 d	27-71d	1-7 d	27-71d
Number of nodes[a]	165	181	211	210	156
Number of edges[b]	769	616	1547	888	1835
Positive edges[c]	435 (56%)	368 (60%)	919 (59%)	493 (56%)	1235 (67%)
Negative edges[d]	334 (43%)	248 (40%)	628 (41%)	395 (44%)	600 (33%)
Modularity[e]	2.96	2.32	1.81	2.78	0.88
Number of communities[f]	26	38	29	58	12
Network diameter[g]	6	9	12	8	6
Average path length[h]	2.95	3.35	3.09	2.99	2.49
Average degree[i]	9.32	6.80	14.66	8.45	23.52
Average clustering coefficient[j]	0.430	0.385	0.449	0.358	0.567

880 [a]Microbial taxon (at genus level) with at least one significant ($P < 0.01$) and strong (SparCC > 0.7 or < -
881 0.7) correlation;
882 [b]Number of connections/correlations obtained by SparCC analysis;
883 [c]SparCC positive correlation (> 0.7 with $P < 0.01$);
884 [d]SparCC negative correlation (< -0.7 with $P < 0.01$);
885 [e]The capability of the nodes to form highly connected communities, that is, a structure with high
886 density of between nodes connections (inferred by Gephi);
887 [f]A community is defined as a group of nodes densely connected internally (Gephi);
888 [g]The longest distance between nodes in the network, measured in number of edges (Gephi);
889 [h]Average network distance between all pair of nodes or the average length off all edges in the
890 network (Gephi);
891 [i]The average number of connections per node in the network, that is, the node connectivity (Gephi);
892 [j]How nodes are embedded in their neighborhood and the degree to which they tend to cluster
893 together (Gephi).
894

895

Figure captions

Figure 1: Methane uptake rate in the un-disturbed and disturbed incubations determined during the pre-incubation, as well as 1-7, 27-34, and 64-71 days interval after desiccation-rewetting. Incubations with ^{13}C- and $^{unlabeled}C$-CH_4 were combined (mean ± s.d., n=6) for each treatment. Pre-incubation is denoted by the shaded area. Significant difference in the methane uptake rate between treatments is indicated by an asterisk (t-test, $p < 0.05$).

Figure 2: Temporal changes in the *pmoA* gene abundance of type Ia (a), type Ib (b), and type II (c) methanotrophs, as determined from group-specific qPCR assays. Each qPCR reaction was performed in duplicate for each DNA extract (n=6), giving a total of 12 replicates per treatment, time, and assay. Pre-incubation is denoted by the shaded area, and dashed lines indicate the detection limit of the qPCR assays. Significant difference in the *pmoA* gene abundance between treatments is indicated by an asterisk (t-test, $p < 0.05$).

Figure 3: Principal component analysis showing the response of the active methanotrophic (a) and bacterial (b) community composition to desiccation-rewetting, as determined from the relative abundances of the *pmoA* and 16S rRNA gene sequences, respectively. Both the *pmoA* and 16S rRNA gene sequences were derived from the ^{13}C-enriched DNA ('heavy' fraction). In (A), the vectors represent the predominant methanotrophs belonging to type Ia (*Methylobacter*), type Ib (RPC, rice paddy cluster), and type II (*Methylocystis*).

Figure 4: The mean active bacterial community composition in the un-disturbed and disturbed incubations, based on the 16S rRNA gene sequence analysis. The 16S rRNA gene sequences

were derived from the ^{13}C-enriched DNA after incubation at 1-7, 27-34, and 64-71 days intervals.

Figure 5: Co-occurence network analysis of the active bacterial community based on the 16S rRNA gene during pre-incubation, and after desiccation-rewetting. The 16S rRNA gene sequences were derived from the ^{13}C-enriched DNA ('heavy' fraction). Samples from 27-34 and 64-71 days intervals were combined to have sufficient replicates for the network analysis; density gradient ultracentrifugation was unsuccessful in 2 of 4 replicated ^{13}C-CH_4 incubations in the disturbed microcosm at 64-71 days interval. Significant ($p < 0.01$) positive (magnitude > 0.7) and negative (magnitude, < -0.7) SparCC correlations are respectively denoted by the blue and red edges. Each node represents a bacterial taxa at the OTU level, and the size of the node corresponds to the number of connections (degree). The colour intensity indicates the betweenness centrality (darker shades indicating higher values). The numbers in the key nodes (top five nodes with highest betweenness centrality) refer to (1) Methylophilaceae, (2) Rhodocyclaceae, (3) *Gemmatirosa*, (4) *Crenothrix* (methane-oxidizer), (5) Acidobacteria subgroup 6, (6) Gemmatimonadaceae, (7) *Methylomonas* (methanotroph), (8) *Noviherbaspirillum*, (9) Beijerinckiaceae, (10) *Paenibacillus*, (11) Acidobacteria subgroup 7, (12) Opitutaceae, (13) Unclassified Bacteria, (14) *Sphingomonas*, (15) Blastocatellia, (16) *Ideonella*, (17) *Chthoniobacter*, (18) Proteobacteria, (19) Chitinophagaceae (20) Microscillaceae. Detailed topological properties of the networks are provided in Table 1.

Table 1: Correlations and topological properties of the interaction networks during pre-incubation, and recovery from desiccation-rewetting at 1 - 7 and 27 - 71 days intervals.

Network properties	Pre-incubation	Un-disturbed		Disturbed	
		1-7 d	27-71d	1-7 d	27-71d
Number of nodes[a]	165	181	211	210	156
Number of edges[b]	769	616	1547	888	1835
Positive edges[c]	435 (56%)	368 (60%)	919 (59%)	493 (56%)	1235 (67%)
Negative edges[d]	334 (43%)	248 (40%)	628 (41%)	395 (44%)	600 (33%)
Modularity[e]	2.96	2.32	1.81	2.78	0.88
Number of communities[f]	26	38	29	58	12
Network diameter[g]	6	9	12	8	6
Average path length[h]	2.95	3.35	3.09	2.99	2.49
Average degree[i]	9.32	6.80	14.66	8.45	23.52
Average clustering coefficient[j]	0.430	0.385	0.449	0.358	0.567

[a]Microbial taxon (at genus level) with at least one significant ($P < 0.01$) and strong (SparCC > 0.7 or < -0.7) correlation;
[b]Number of connections/correlations obtained by SparCC analysis;
[c]SparCC positive correlation (> 0.7 with $P < 0.01$);
[d]SparCC negative correlation (< -0.7 with $P < 0.01$);
[e]The capability of the nodes to form highly connected communities, that is, a structure with high density of between nodes connections (inferred by Gephi);
[f]A community is defined as a group of nodes densely connected internally (Gephi);
[g]The longest distance between nodes in the network, measured in number of edges (Gephi);
[h]Average network distance between all pair of nodes or the average length off all edges in the network (Gephi);
[i]The average number of connections per node in the network, that is, the node connectivity (Gephi);
[j]How nodes are embedded in their neighborhood and the degree to which they tend to cluster together (Gephi).

Figure 1

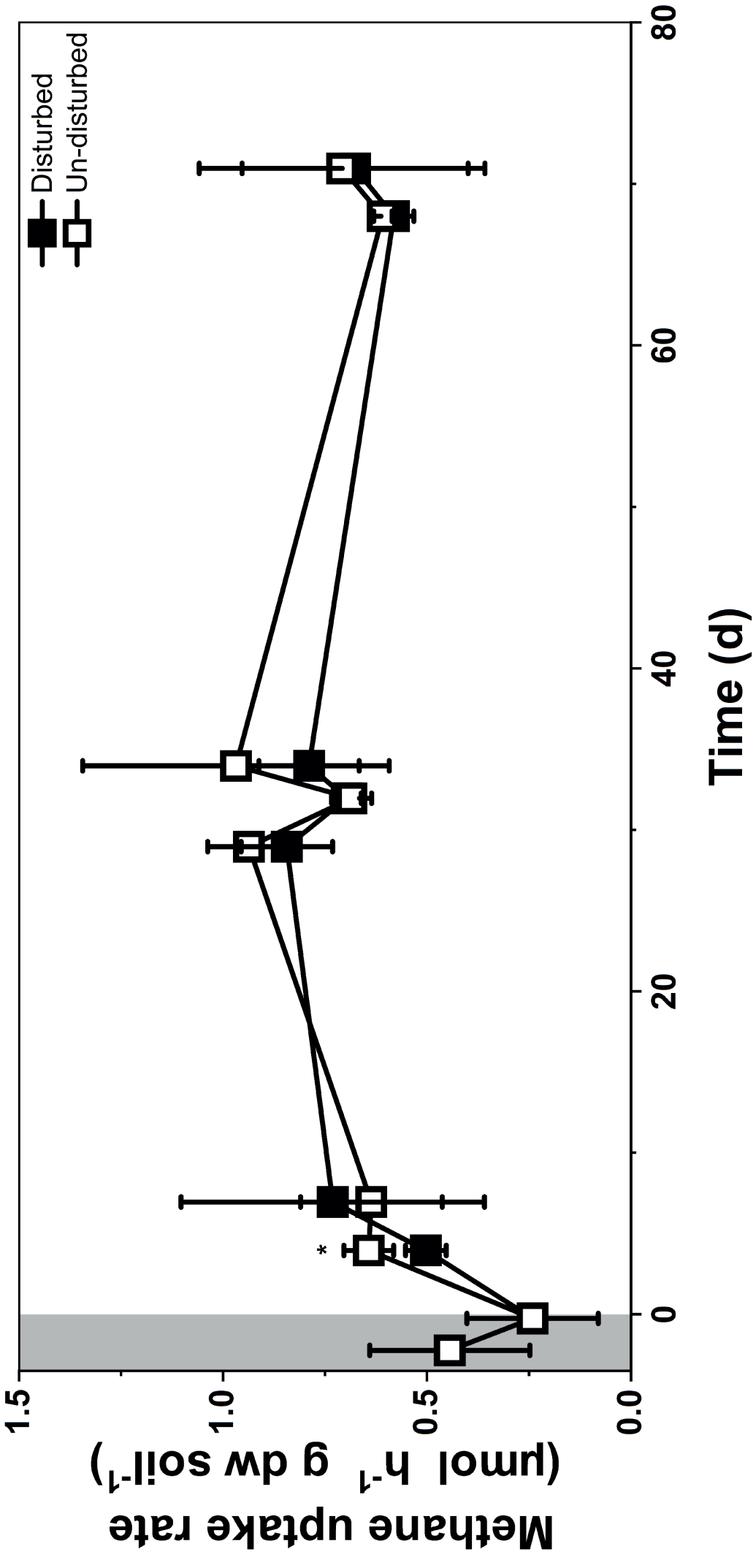
Disturbed
Un-disturbed
*
0.0
0.5
1.0
1.5
0
20
40
60
80
Time (d)
Methane uptake rate
(μmol h-1 g dw soil-1)

Figure 2

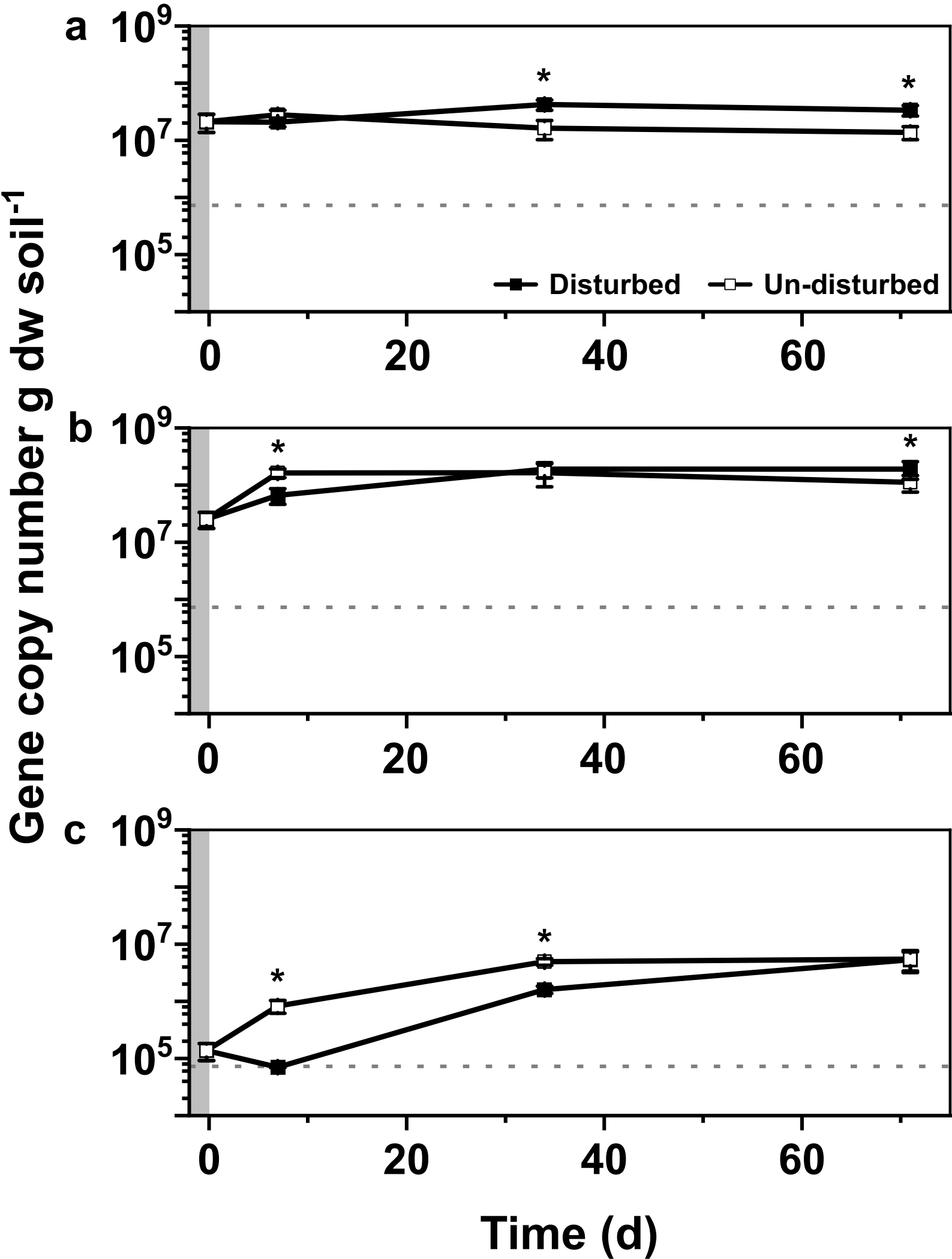
a
b
c
10^9
10^7
10^5
*
Disturbed
Un-disturbed
0
20
40
60
Gene copy number g dw soil^{-1}
Time (d)

Figure 3

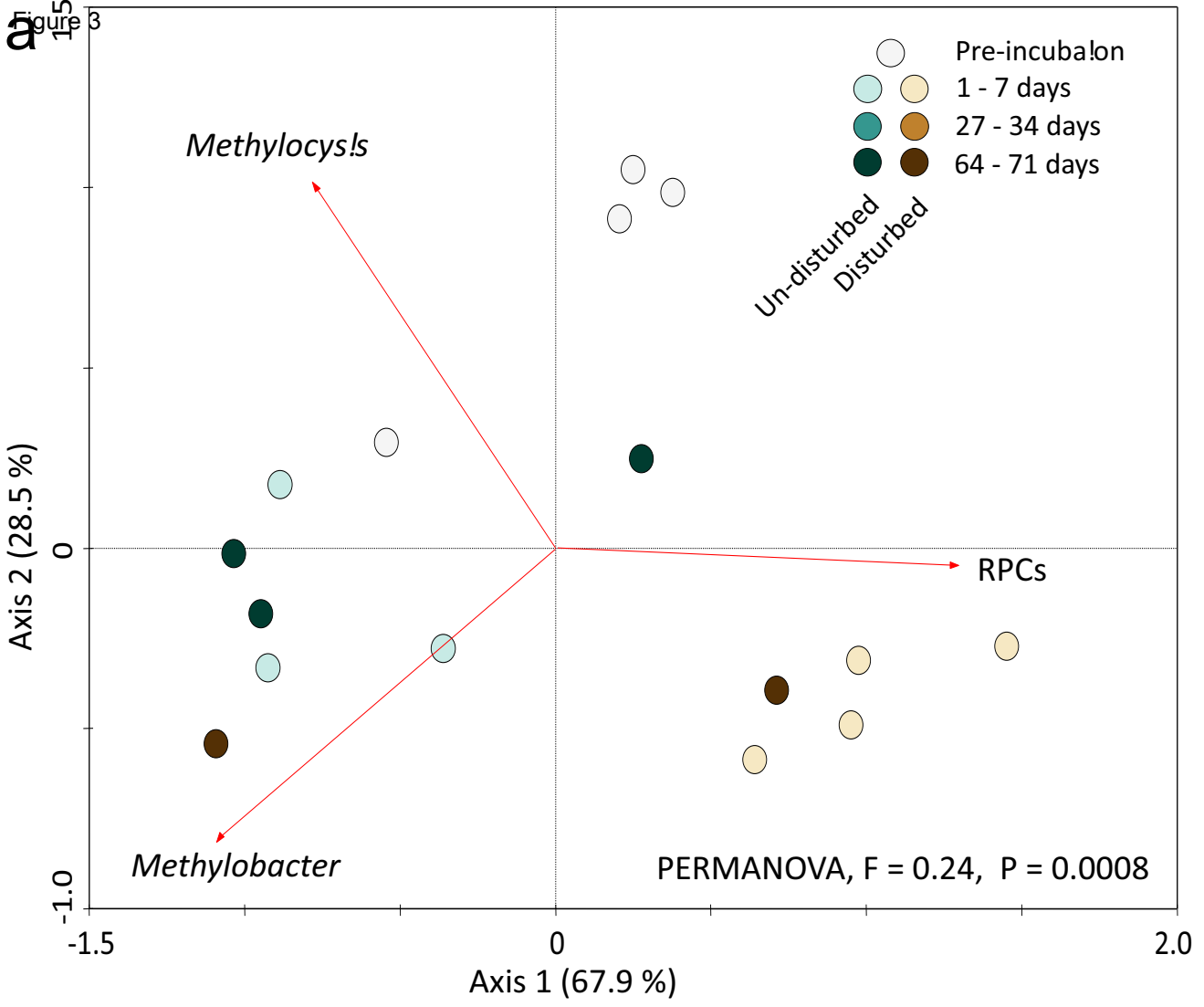
a
Pre-incubation
1 - 7 days
27 - 34 days
64 - 71 days
Un-disturbed
Disturbed
Methylocystis
RPCs
Methylobacter
PERMANOVA, F = 0.24, P = 0.0008
Axis 2 (28.5 %)
Axis 1 (67.9 %)
1.5
0
-1.0
-1.5
0
2.0

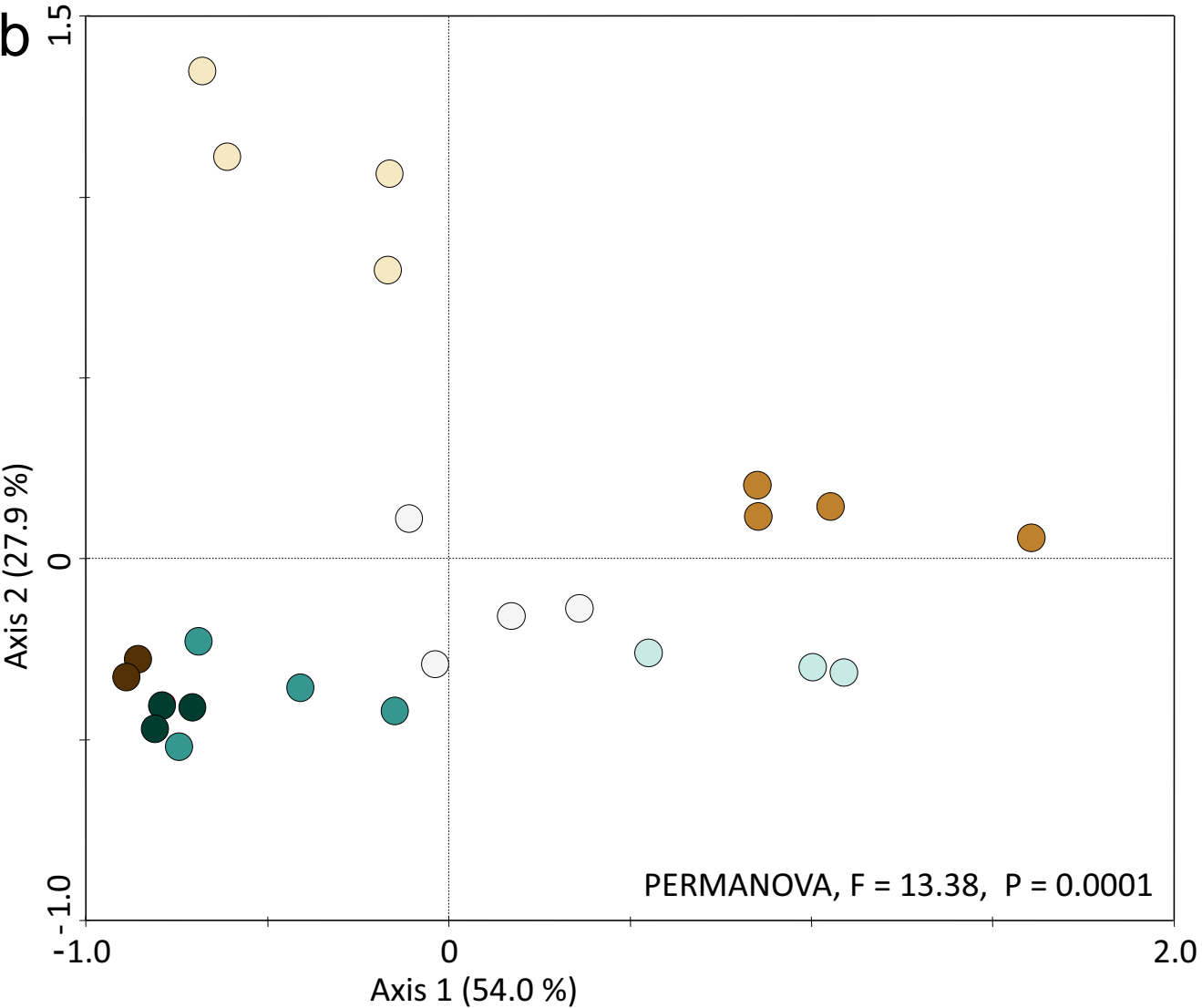
b
PERMANOVA, F = 13.38, P = 0.0001
Axis 2 (27.9 %)
Axis 1 (54.0 %)
1.5
0
-1.0
-1.0
0
2.0

Figure 4

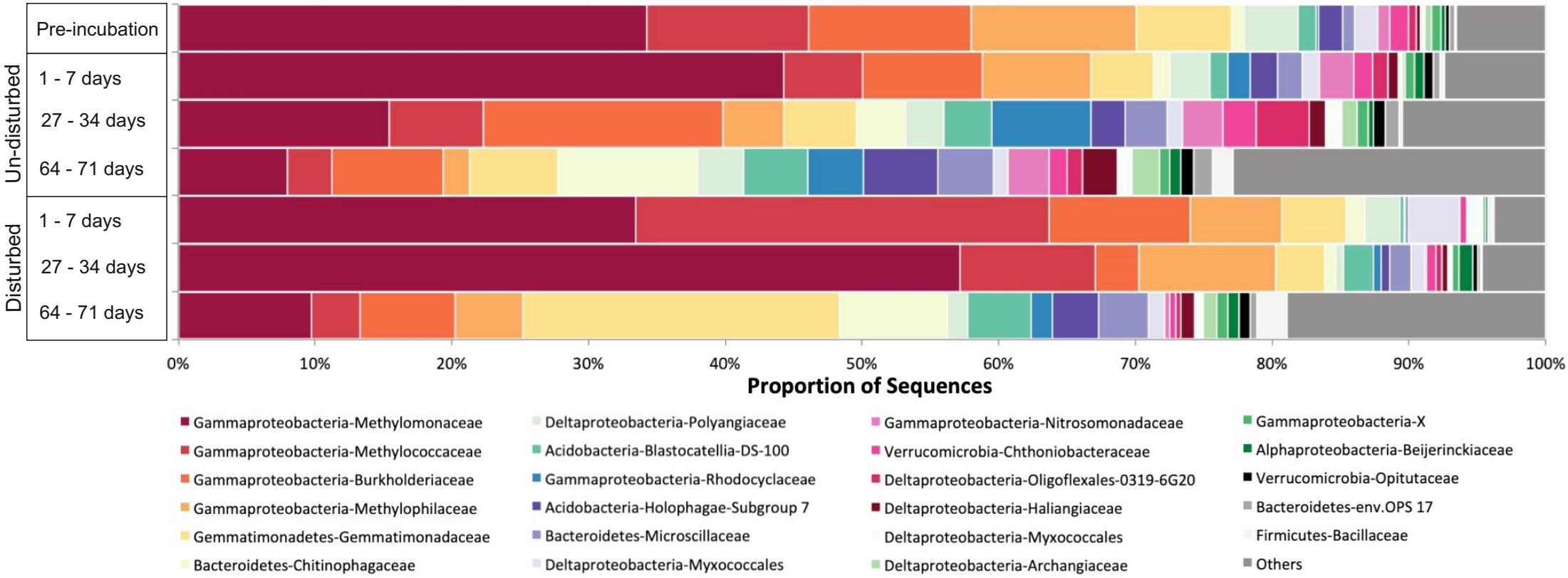
Pre-incubation
Un-disturbed
1 - 7 days
27 - 34 days
64 - 71 days
Disturbed
1 - 7 days
27 - 34 days
64 - 71 days
0%
10%
20%
30%
40%
50%
60%
70%
80%
90%
100%
Proportion of Sequences
Gammaproteobacteria-Methylomonaceae
Gammaproteobacteria-Methylococcaceae
Gammaproteobacteria-Burkholderiaceae
Gammaproteobacteria-Methylophilaceae
Gemmatimonadetes-Gemmatimonadaceae
Bacteroidetes-Chitinophagaceae
Deltaproteobacteria-Polyangiaceae
Acidobacteria-Blastocatellia-DS-100
Gammaproteobacteria-Rhodocyclaceae
Acidobacteria-Holophagae-Subgroup 7
Bacteroidetes-Microscillaceae
Deltaproteobacteria-Myxococcales
Gammaproteobacteria-Nitrosomonadaceae
Verrucomicrobia-Chthoniobacteraceae
Deltaproteobacteria-Oligoflexales-0319-6G20
Deltaproteobacteria-Haliangiaceae
Deltaproteobacteria-Myxococcales
Deltaproteobacteria-Archangiaceae
Gammaproteobacteria-X
Alphaproteobacteria-Beijerinckiaceae
Verrucomicrobia-Opitutaceae
Bacteroidetes-env.OPS 17
Firmicutes-Bacillaceae
Others

Figure 5

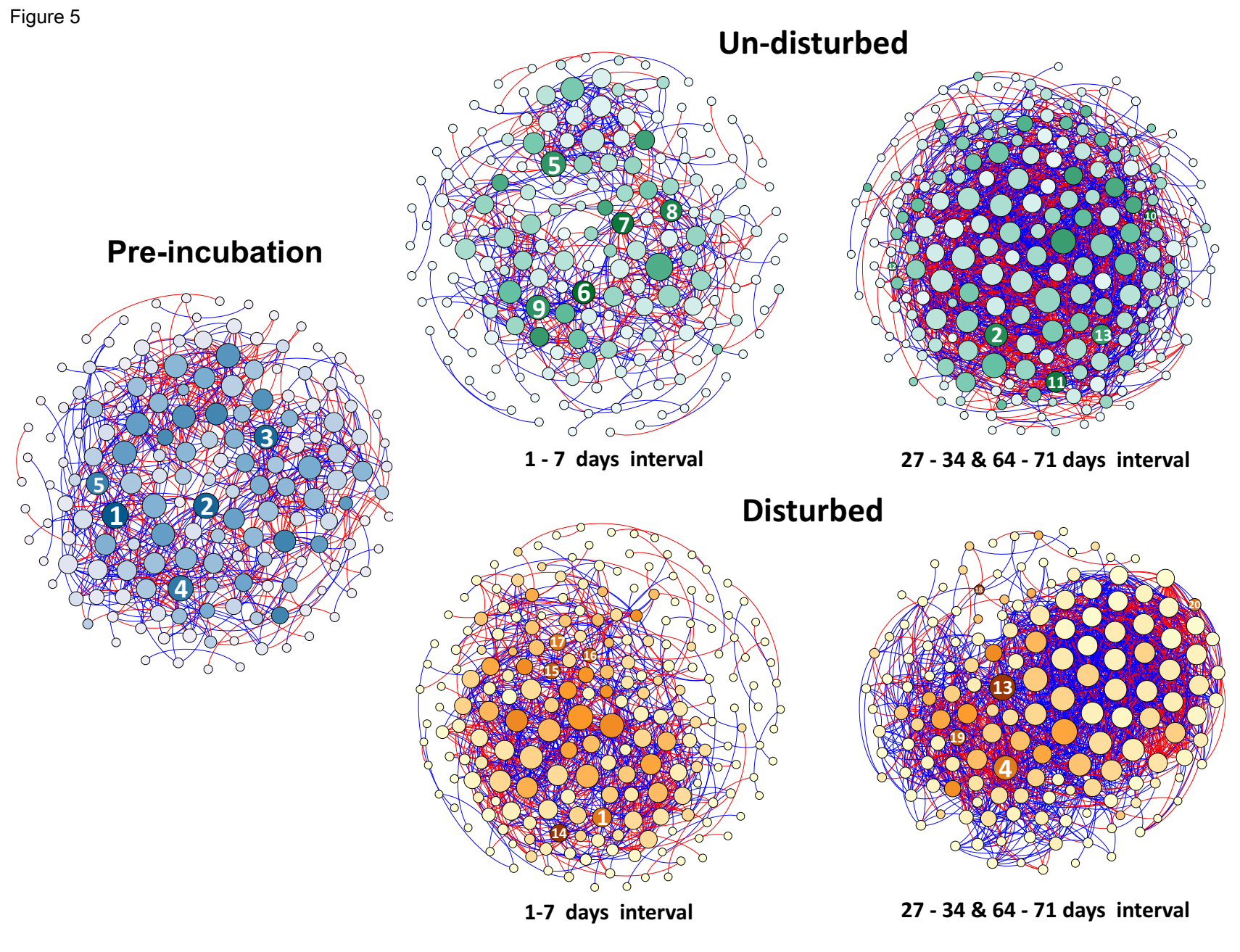
Un-disturbed
Pre-incubation
1 - 7 days interval
27 - 34 & 64 - 71 days interval
Disturbed
1-7 days interval
27 - 34 & 64 - 71 days interval